PAPER

Check for updates

Cite this: *RSC Adv.*, 2019, **9**, 14701

Effect of size of latex particles on the mechanical properties of hydrogels reinforced by latex particles

Li Liu,[ab] Guangchao Lv,[ab] Xiuyan Ren, [ID][ab] Xinhe Li,[ab] Te Wang,[ab] Jingwen Dong,[ab] Zeyu Wang[ab] and Guangfeng Wu [ID] *[ab]

Herein, cationic latex particles (CL) of different particle sizes were introduced as a cross-linking center to enhance the mechanical properties of the hydrophobically-associated hydrogels (P(AAm-*co*-HMA)-CL). Firstly, cationic polymethylmethacrylate (PMMA) latex particles were synthesized *via* soap-free emulsion polymerization. Subsequently, P(AAm-*co*-HMA)-CL hydrogels with outstanding mechanical properties were prepared using acrylamide as the monomer, hexadecyl methacrylate as the hydrophobic molecule, and CL as the cross-linking center. The size of CL had a significant effect on the mechanical properties and self-recovery properties of the P(AAm-*co*-HMA)-CL hydrogels. The hydrogel with larger CL size exhibited low mechanical properties due to weak hydrophobic interactions. In contrast, the hydrogel with small CL size displayed excellent mechanical properties due to an effective entanglement of the hydrophobic chains with the smaller size CL, which significantly affects the mechanical properties of the hydrogel. As a result, the maximum fracture stress and fracture strain of the hydrogel were up to 1.47 MPa and 2847%, respectively. This study can have a profound impact on the development of the technology of toughening hydrogels with latex particles.

Introduction

Polymer hydrogels are soft and wet smart biomaterials that consist of a three-dimensional network and a large amount of water.[1] Significant attention has been paid to hydrogels due to their promising applications in the biomedical area,[2] such as cartilage substitute,[3,4] drug delivery,[5] and tissue engineering.[6,7] However, poor mechanical properties of chemically cross-linked conventional hydrogels limit their applications. Therefore, enhancing the mechanical properties of hydrogels has attracted a great number of researchers. Recently, several strategies have been developed to increase the mechanical properties of hydrogels, such as nanocomposite hydrogels,[8–10] slide-ring hydrogels,[11] tetra-PEG hydrogels,[12,13] macromolecular microspheres composite (MMC) hydrogels,[14,15] and double network (DN) hydrogels.[16–18]

Macromolecular microspheres play an important role in the polymeric materials. Consequently, macromolecular microspheres composite (MMC) hydrogels have also become important hydrogels with high mechanical strength. Wang *et al.*[19] prepared MMC hydrogels using ⁶⁰Co γ-ray irradiation, wherein a peroxidized MMS acted as both a crosslinker and an initiator. The grafted PAA chains on the neighboring MMSs can be

chemically bonded and some can even entangle each other. Wu *et al.*[20] fabricated nanoparticle composite polyacrylamide (PAAm) hydrogels using *in situ* free-radical polymerization with crosslinked polystyrene (PS) nanoparticles. All the MMC hydrogels exhibited excellent compressive properties but not impressive tensile strength due to the presence of chemical crosslinkers. Ren *et al.*[21] first improved the mechanical properties of the hydrogels using core–shell latex particles in combination with physical hydrophobic-association interactions. In the presence of a surfactant, the core–shell latex particles interact effectively with a large number of hydrophobic segments. When hydrogels are subjected to an external force, the curled hydrophobic chains can slide, extend, and disentangle along with the deformation of micelles, dissipating extensive energy in the process. On this basis, their group investigated the effects of different types of latex particles on the mechanical properties of hydrophobically-associated hydrogels. Xia[22] introduced the core–shell inorganic–organic hybrid latex particles (SiO₂-*g*-PBA) as hydrophobic cross-linking centers to prepare the hydrophobically-associated hydrogels. When the hydrogel was impacted by the external forces, the inorganic SiO₂ core could maintain the spherical shape and the hydrophobic chains in the organic PBA shell could dissipate energy. These hydrogels not only had high mechanical properties but also good resistance properties. Gu[23] used the cationic PS latex as the hydrophobic cross-linking centers to prepare the hydrophobically-associated hydrogels. The cationic latex with cationic group could absorb the anionic initiator *via*

[a]*Engineering Research Center of Synthetic Resin and Special Fiber, Ministry of Education, Changchun University of Technology, Changchun, PR China. E-mail: gfwu20@163.com; Fax: +86-431-85716467; Tel: +86-431-85716467*

[b]*School of Chemical Engineering, Changchun University of Technology, Changchun, PR China*

electrostatic interactions. Therefore, the cationic latex apart from acting as the hydrophobic-association centers also acted as the ionic crosslinking centers, leading to the improvement of tensile and compression strength of cationic latex composite hydrogels. Their group also introduced macromolecular microspheres as the cross-linking centers for the hydrophobic association in the double-network hydrogels. Hou[24] prepared the double-network hydrogels with gelatin as the first network and copolymer of acrylamide and hexadecyl methacrylate stabilized with macromolecular microspheres (PBA) as the second network. These hydrogels also exhibited outstanding mechanical properties. These studies show that different latex particles as the hydrophobic cross-linking points could effectively toughen the hydrogels. In addition to these studies, they investigated the effect of hydrophobic alkyl chain length on the mechanical properties of the hydrophobically-associated hydrogels. Gao[25] selected different long alkyl chains as segments to enhance the performance of the hydrophobically-associated hydrogels with the PBA latex particles as the cross-linking centers. Hence, the long alkyl chains could effectively entangle with the PBA latex particles through strong hydrophobic interactions. However, till date, the effect of latex particle sizes on the hydrophobically-associated hydrogels had not been investigated. We hypothesized that the latex particle size could exert a great influence on the hydrophobic interaction and affect the mechanical properties of hydrogel.

In this work, cationic PMMA latex particles (CL) with different particle sizes were synthesized and introduced as cross-linking centers to enhance the mechanical properties of the hydrophobically-associated hydrogel (P(AAm-*co*-HMA)-CL). Effect of CL size on the mechanical properties of hydrogels was measured through tensile test, loading–unloading cyclic test, and successive cycling tests. Subsequently, rheological performance of the hydrogels with different size of cationic latex particles was also investigated. The results can promote the development of hydrogels toughened with latex particles.

Experimental

Materials

Acrylamide (AAm) was purchased from Macklin, while methyl methacrylate (MMA), [2-(methacryloyloxy)ethyl]trimethylammonium chloride (MATMAC was 80% aqueous solution), 2,2′-azobis(2-amidinopropane)dihydrochloride (V50), potassium persulfate(KPS), hexadecyl methacrylate (HMA), *N*,*N*,*N*′,*N*′-tetramethylethylenediamine (TMEDA), *N*,*N*′-methylene-bis-acrylamide (MBA), cetyltrimethylammonium bromide (CTAB), and sodium chloride (NaCl) were purchased from Aladdin. Deionized water was used to prepare all the solutions.

Synthesis of cationic PMMA latex particles

The soap-free emulsion polymerization was carried out in a 250 ml three-necked flask fitted with a re-flux condenser, stirrer, and nitrogen inlet tube. Firstly, H_2O and MMA were added to the three-necked flask and stirred for 20 min at 300 rpm. Subsequently, the cationic monomer MATMAC and

cross-linking agent MBA were added and system was stirred for 10 min. Finally, initiator V50 was added to start the reaction and the reaction was allowed to run for 4 h. After polymerization, the latex with cationic PMMA latex particles and 7% solid content was obtained. All the recipes and experimental conditions for the polymerization reaction are presented in Table 1.

Synthesis of hydrogels

P(AAm-*co*-HMA)-CL hydrogels were toughened by cationic PMMA latex particles (CL). P(AAm-*co*-HMA)-CL hydrogels were formed *via* copolymerization of AAm and HMA and introduction of cationic PMMA latex particles with different sizes(192 nm, 226 nm, 291 nm, 337 nm) as the hydrophobic cross-linking centers. In brief, CTAB (3 g) and NaCl (0.87 g) were dissolved in 30 ml deionized water to obtain the SDS/NaCl aqueous solution. Then, CL (0 wt%, 0.1 wt%, 0.2 wt%, 0.25 wt%, 0.3 wt% to AAm) and HMA (0 mol%, 1 mol%, 3 mol%, 5 mol%, 7 mol% to AAm) were added into the system with speed stirring for 24 h at 25 °C to maintain the stability and dispersion of the hydrophobic segments. Subsequently, the monomer AAm (9 g) and initiator KPS (0.03 g) were added to the reaction vessel. Finally, TMEDA (45 μL) was added to the system at the speed stirring for 2 min. All the solutions were transferred into a mold composed of two glass plates with a 2 mm thick silicone rubber and placed at 50 °C for 24 h to obtain P(AAm-*co*-HMA)-CL hydrogels.

Characterization

DLS measurement. The diameter and size distribution of cationic PMMA latex particles were measured using dynamic light scattering (DLS) instrument (American Brookhaven 90 plus Particle Size Analyzer). The laser light-scattering measurement was set at 90°. Multiple tests were conducted for each sample and then the effective diameter and size distribution were determined.

FTIR spectrometric analysis. The chemical structure of cationic PMMA latex particles was analyzed *via* FTIR spectroscopy using a Nicolet iS-50 FTIR spectrometer at the resolution of 4 cm^{-1} and 64 cm^{-1} scans for each sample. Before tests, the samples were freeze-dried under vacuum in a freeze.

TEM measurements. To determine the morphologies of the cationic PMMA latex particles, a transmission electron microscope (TEM) was used at an accelerating voltage of 100 kV. Firstly, the samples were prepared by diluting the dispersion in water. Then one droplet of the diluted samples was placed on

Table 1 The recipes and experimental conditions for the polymerizations

Code	$CL_{192\ nm}$	$CL_{226\ nm}$	$CL_{291\ nm}$	$CL_{337\ nm}$
MMA (g)	15	15	15	15
MATMAC (g)	1.5	1.5	1.5	1.5
V50 (g)	0.15	0.15	0.18	0.15
MBA (g)	0.028	0.028	0.028	0.028
H_2O (g)	150	150	150	150
T (°C)	85	75	70	70

a carbon-coated copper grid and dried at room temperature for observation.

Gel fraction (gel%) test. First, the hydrogel samples were freeze-dried and weighed. At this time, the dry weight of the hydrogel samples were recorded as W_0. Then the dried hydrogel samples were immersed in distilled water and the distilled water was replaced regularly. When the samples achieved swelling equilibrium, the samples were freeze-dried and the dry weight were recorded as W_d, gel% = $W_d/W_0 \times 100\%$.

Mechanical tests. The mechanical properties of hydrogels were measured through a tensile tester (SHIMADZU, model AGS-X, 100N, Japan) at the room temperature. Dumbbell-shaped samples were prepared by cutting tools with a length of 30 mm, a gauge length of 12 mm, a width of 4 mm, and a thickness of 2 mm. The rate of stretching was fixed at 80 mm min^{-1}. The fracture energy (toughness) was calculated by integrating the area underneath the stress–strain curve of the hydrogel samples.

For tensile loading–unloading cyclic tests, the samples were stretched to a pre-set strain (1000%) and then returned to the initial length. The rate of stretching was fixed at 100 mm min^{-1}. The dissipated energy of the samples was determined from the area between the loading–unloading curves. For the successive tensile cycling tests without any rest time, the samples were first stretched to a strain of 1000% and then unloaded. The rate of stretching was fixed at 100 mm min^{-1}.

Rheological tests. Dynamic rheological measurements were performed with Anton Paar MCR 302 rheometer at 25 °C using 25 mm flat parallel plates. Dynamic oscillatory strain sweep experiments were performed on the hydrogels to determine the limit of the linear viscoelastic region. The dynamic strain sweep from 0.1% to 100% was first performed at a constant frequency, $\omega = 10$ rad s^{-1}. Then, strain recovery tests were performed at $\gamma = 0.01\%$. Consequently, frequency sweep tests were performed at a strain amplitude of $\gamma = 1\%$ over a frequency range of 0.01 rad s^{-1} to 100 rad s^{-1} for all the samples.

Results and discussion

The cationic PMMA latex particles were synthesized *via* non-soap emulsion polymerization. The obtained cationic PMMA latex particles were characterized by FTIR spectra in Fig. 1. In the curve of pure PMMA, the strong band at 1730 cm^{-1} can be attributed to the stretching vibration of C=O band and the peak at 1450 cm^{-1} can be attributed to the bending vibration of C–O band. Compared to the curve of pure PMMA, there was a novel peak in the curve of cationic PMMA latex particles at 1630 cm^{-1} that can be assigned to the stretching vibration of C–N band. The result of FTIR spectra confirmed that the reaction was successful. The TEM image and particle size distribution of cationic PMMA latex particles are shown in Fig. 2. The cationic PMMA latex particles exhibited uniform spherical shapes and smooth surfaces. The particle size distribution images displayed a single peak with a narrow distribution and the mean diameter were 192 nm, 226 nm, 291 nm, and 337 nm, respectively. The cationic PMMA latex particles had good monodispersity.
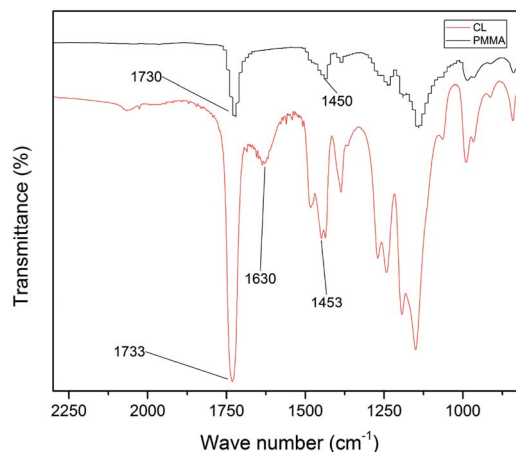

Fig. 1 FTIR spectroscopy of CL and PMMA latex particles.

The hydrogels were synthesized through the radical polymerization of AAm and HMA in the presence of CL with different sizes. The gel fraction of the hydrogel samples with different sizes of CL (192 nm, 226 nm, 291 nm and 337 nm) were presented in Table 2. In the Table 2, the gel fraction of the hydrogel samples were above 70% which means that the monomer entered the polymer network at 70% and the experiment successfully prepared the hydrogels. In addition, since the network of hydrogels were physically crosslinked, de-crosslinking would occur during the swelling process, so the ratio of monomers actually entering the polymer network should be larger than 70%.

To study the toughening effect of hydrogels, the typical tensile stress–strain curve of PAAm-CL hydrogel, P(AAm-co-HMA) hydrogel, and P(AAm-co-HMA)-CL hydrogel are presented in Fig. 3. It is evident that P(AAm-co-HMA)-CL hydrogel possessed significantly better mechanical performance than
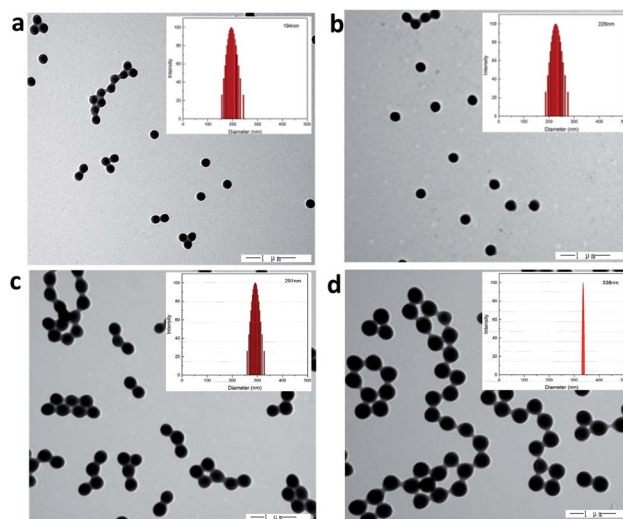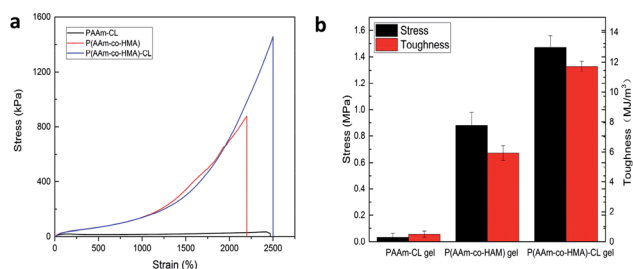

Fig. 2 The TEM images and size distribution of CL latex particles with different diameter ((a) CL$_{194\ nm}$, (b) CL$_{226\ nm}$, (c) CL$_{291\ nm}$, (d) CL$_{337\ nm}$ and the PDI were 0.018, 0.014, 0.005 and 0.005 respectively).
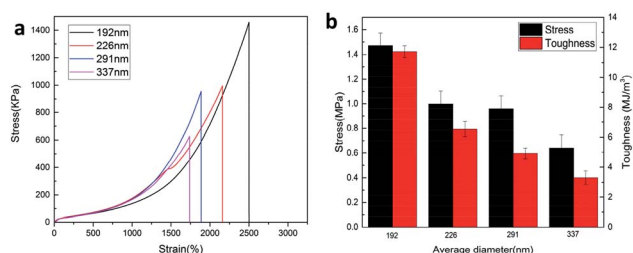
Table 2 The gel fraction of the samples with different sizes of CL (192 nm, 226 nm, 291 nm and 337 nm)

Code	P(AAm-*co*-HMA)-CL$_{192\ nm}$	P(AAm-*co*-HMA)-CL$_{226\ nm}$	P(AAm-*co*-HMA)-CL$_{291\ nm}$	P(AAm-*co*-HMA)-CL$_{337\ nm}$
W_0 (g)	0.393	0.391	0.319	0.396
W_d (g)	0.277	0.277	0.224	0.278
Gel (%)	70.48	70.84	70.22	70.20

Fig. 3 (a) Tensile curve and (b) toughness of PAAm-CL hydrogel, P(AAm-*co*-HMA) hydrogel and P(AAm-*co*-HMA)-CL hydrogel.

PAAm-CL hydrogel and P(AAm-*co*-HMA) hydrogel. The tensile strength and toughness of PAAm-CL hydrogel were 0.034 MPa and 0.51 MJ m^{-3} and the tensile strength and toughness of P(AAm-*co*-HMA) hydrogel were 0.88 MPa and 5.93 MJ m^{-3}. In contrast, the tensile strength of P(AAm-*co*-HMA)-CL hydrogel could reach up to 1.47 MPa and 11.72 MJ m^{-3}. The tensile strength of P(AAm-*co*-HMA)-CL hydrogel was approximately 40 times higher than that of PAAm-CL hydrogel and two times higher than that of P(AAm-*co*-HMA) hydrogel, respectively. Due to the absorption of hydrophobic segments into CL as a dynamic cross-linking center, the strength and toughness of P(AAm-*co*-HMA) hydrogels were clearly enhanced.
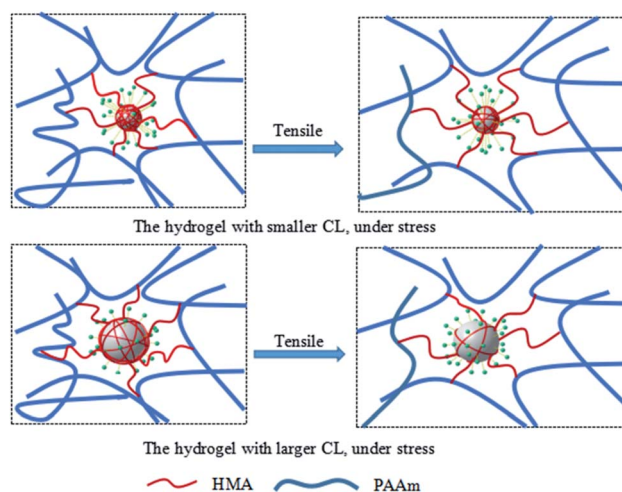
The effect of the CL size on the mechanical properties of the P(AAm-*co*-HMA)-CL hydrogels was investigated. The typical tensile stress–strain curves of P(AAm-*co*-HMA)-CL hydrogel with different sizes of CL are shown in Fig. 4. It is evident that P(AAm-*co*-HMA)-CL$_{(194\ nm)}$ hydrogels displayed great mechanical performance. While the fracture stress, fracture strain, and toughness of P(AAm-*co*-HMA)-CL hydrogels were decreased as the size of CL increased. These results are due to the small size of latex particles facilitating the tangling of hydrophobic segments on their surface. The degree of entanglement of the

hydrophobic chains on the surface of smaller CL was stronger than that for the larger one. When the hydrogels were subjected to an external force, the hydrophobic segments on the surface of the large CL were easy to disentangle.

The toughening mechanism of the P(AAm-*co*-HMA)-CL hydrogels with different sizes of CL is proposed in Fig. 5. In the case of P(AAm-*co*-HMA)-CL hydrogels with larger CL, the hydrophobic chains were prone to disentangle from CL under the subject of external forces as the degree of entanglement of the hydrophobic segment was lower. Therefore, the network was easy to destroy, resulting in the poor mechanical properties of hydrogel. In the case of the P(AAm-*co*-HMA)-CL hydrogels with smaller CL, the hydrophobic chains were hardly disentangled from CL as the degree of entanglement of the hydrophobic segments was stronger. Under external forces, some hydrophobic chains disentangled from CL and other hydrophobic chains could only transform from curling to stretching. Therefore, the hydrogels exhibited stronger mechanical properties.

A general principle for the design of tough hydrogels is implementing the mechanisms into hydrogels to dissipate significant amounts of mechanical energy.[26] In order to investigate the energy dissipation behavior of the P(AAm-*co*-HMA)-CL hydrogels with different sizes of CL, the hysteresis behavior of the hydrogels during the loading–unloading cycle was investigated. Fig. 6 shows the negligible hysteresis loop of stress–strain curve and energy dissipation for P(AAm-*co*-HMA)-CL hydrogels with different sizes of CL at a strain of 1000%. P(AAm-*co*-LMA)-

Fig. 4 (a) Tensile curve and (b) toughness of P(AAm-*co*-HMA)-CL hydrogel with different size of CL.

Fig. 5 The toughening mechanism for P(AAm-*co*-HMA)-CL hydrogels with different size of CL.
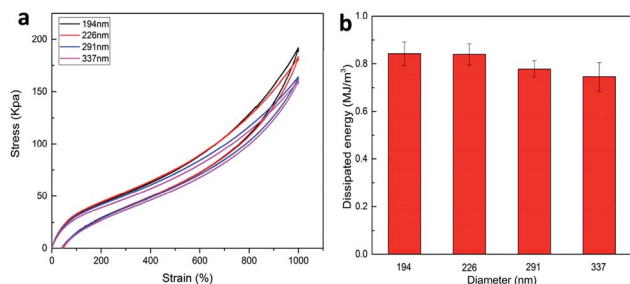
Fig. 6 (a) Loading−unloading cycle behaviors of P(AAm-*co*-HMA)-CL hydrogels with different size of CL; (b) dissipated energy from (a).

$CL_{(194\ nm)}$ hydrogel displayed a substantial increase in the hysteresis loop as compared to the other hydrogels. The total energy and dissipated energy of P(AAm-*co*-HMA)-$CL_{(194\ nm)}$ hydrogels was higher than that for the other three P(AAm-*co*-HMA)-CL hydrogels with larger size of CL. The results indicate that by using a smaller size CL as the crosslinking center for hydrophobic segments, there was effective energy dissipation, and the hydrogels exhibited outstanding toughness. These results also prove that smaller size latex particles facilitated the tangling of hydrophobic segments on their surface. Therefore, P(AAm-*co*-LMA)-$CL_{(194\ nm)}$ hydrogels exhibited excellent mechanical properties.

Furthermore, in the case of P(AAm-*co*-LMA)-$CL_{(194\ nm)}$ hydrogels, successive tensile loading–unloading curves without any rest time were investigated. As shown in Fig. 7, a distinct hysteresis loop was observed for the first loading–unloading cycle of P(AAm-*co*-HMA)-$CL_{(194\ nm)}$ hydrogel, indicating that the hydrogel could effectively dissipate energy. When the last three cycles were carried out immediately after the first one the last three cycles were almost elastic with the hysteresis loop of small size. The dissipated energy in the last three cycles could only recover to about 30% of its original value. But the dissipated energy in the last cycle was higher than the second and third cycles, indicating that the disentangled chains during the first three loading processes rearranged in the following testing process. The recovery process is time dependent due to the recombination of physical cross-linking structures in the hydrogels.[23,27] As a result, the P(AAm-*co*-HMA)-$CL_{(194\ nm)}$ hydrogel displayed excellent resilience and anti-fatigue performance.
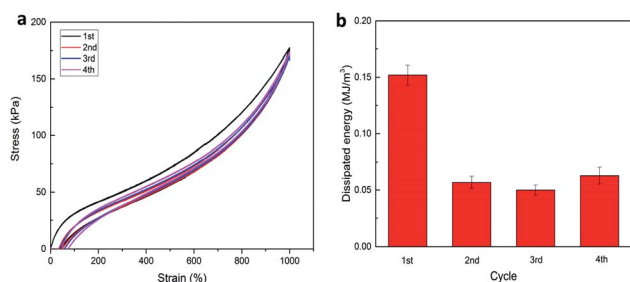
Rheological characterization is an effective method to analyze the variety of internal structure of hydrogels. The dynamic rheology behavior of the P(AAm-*co*-HMA)-CL hydrogels with different sizes of CL is presented in Fig. 8. In Fig. 8a, a significant strain-dependent viscoelastic response could be observed. In the linear viscoelastic region of γ from 0.1% to 1%, G' of P(AAm-*co*-HMA)-$CL_{(194\ nm)}$ hydrogel was lower than that of the P(AAm-*co*-HMA)-$CL_{(226\ nm)}$ hydrogel but higher than those of the P(AAm-*co*-HMA)-$CL_{(291\ nm)}$ hydrogel and P(AAm-*co*-HMA)-$CL_{(337\ nm)}$ hydrogel. The bigger size of CL had a higher modulus; therefore, G' of P(AAm-*co*-HMA)-$CL_{(194\ nm)}$ hydrogel was lower than that of the P(AAm-*co*-HMA)-$CL_{(226\ nm)}$ hydrogel. While the size of CL was extremely large, the association of the hydrophobic segment was weakened and the mechanical properties of the hydrogels became weak. And in the range of 1% to 100%, the hydrogels exhibited nonlinear viscoelastic behavior and G' were decreased significantly, though the G' of P(AAm-*co*-HMA)-$CL_{(194\ nm)}$ decreased relatively slowly. The intersections of G' and G'' were the gel points of the hydrogels as shown in Fig. 8b. The strain value at the gel point decreased as the size of CL increased. This phenomenon indicates that the network structure of P(AAm-*co*-HMA)-$CL_{(194\ nm)}$ hydrogel was not easily damaged by the shear strain because the smaller size of latex particles facilitated the tangling of hydrophobic segments on their surface.

After the shear strain test, we also performed the time recovery test and the results are shown in Fig. 8c and c'. The recovery rate of P(AAm-*co*-HMA)-$CL_{(194\ nm)}$ hydrogel was significantly faster than those of the other three hydrogels. When the recovery time was 300 s, the recovery rate of P(AAm-*co*-HMA)-CL hydrogels with different sizes of CL were 82.29%, 80.37%, 77.11%, and 76.79%, respectively. The recovery rate of P(AAm-*co*-HMA)-CL hydrogels decreased significantly as the size of CL
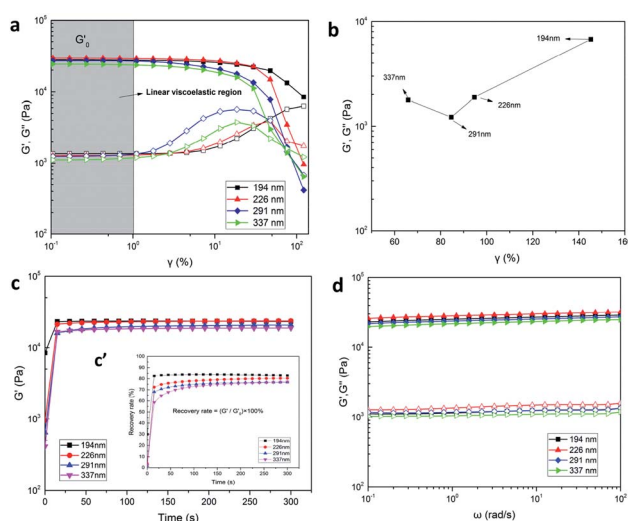

Fig. 7 (a) Successive loading−unloading curves of P(AAm-*co*-HMA)-$CL_{(194\ nm)}$ hydrogel, (b) dissipated energy from (a).

Fig. 8 (a) Storage modulus (G') and loss modulus (G'') of P(AAm-*co*-HMA)-CL with different CL size of shear strain test, (b) gel points from (a), (c) time recovery test and (c') recovery rate, (d) storage modulus (G') and loss modulus (G'') of P(AAm-*co*-HMA)-CL with different CL size of frequency sweeping test (ω = 10 rad s^{-1}).

increased. These results indicate that smaller size of CL was more conducive to the hydrophobic chains entanglement; and hence, these hydrogels had good self-recovery properties. Additionally, G' and G'' were also measured at different frequency sweeps (see Fig. 8d). The storage modulus G' was higher than the loss modulus G'' in the above-mentioned frequency range. G' and G'' were slightly dependent on frequency, suggesting that all hydrogels almost had no dissociation. Moreover, G' of P(AAm-co-HMA)-CL$_{(226\ nm)}$ hydrogel was higher than that of the P(AAm-co-HMA)-CL$_{(194\ nm)}$ hydrogel as the bigger size of CL led to a higher modulus. Subsequently, G' was decreased as the size of CL increased. When the size of CL was extremely large, the association of the hydrophobic segments was weakened. In this case, the CL is equivalent to an organic filler in the hydrogel which makes the mechanical properties of the hydrogel decrease. The results of G' shown in Fig. 8d were same as those shown in Fig. 8a. Appropriate sizes of latex particles were conducive to hydrophobic chain entanglement and it was possible to simultaneously improve the strength and toughness of the hydrogels. Therefore, it is necessary to choose the right size of latex particles.

Subsequently, the influence of CL content and HMA/AAm molar ratio on the mechanical properties of P(AAm-co-HMA)-CL hydrogel were investigated. The typical stress–strain curves are shown in Fig. 9. In Fig. 9a and b, it is evident that the tensile strength and toughness of P(AAm-co-HMA)-CL hydrogels increased considerably with increasing CL contents from 0 to 0.25 wt% and then decreased at the CL content of 0.3 wt%. CL as the dynamic hydrophobic crosslinking centers could redistribute the stress via disentanglement from hydrophobic segments. Therefore, the mechanical properties of the P(AAm-co-HMA)-CL hydrogels increased as the CL content increased. However, at the CL content of 0.3 wt%, excessive cross-linking

reduced the mechanical properties of P(AAm-co-HMA)-CL hydrogels. As shown in Fig. 9c and d, the tensile strength and toughness of P(AAm-co-HMA)-CL hydrogels increased with increasing HMA content from 0 to 5 mol%, and then decreased at the HMA content of 7 mol%. The plausible reason for the observation could be that with the increase of HMA/AAm molar ratio, more HMA chains interacted with CL to form ionic crosslinking and hydrophobic associations. These interactions led to a growth of crosslinking points in the network resulting in enhancing the tensile strength and toughness of P(AAm-co-HMA)-CL hydrogels. However, an excessive increase in HMA/AAm molar ratio also resulted in the P(AAm-co-HMA)-CL hydrogel with excessive crosslinked networks. As a result, the mechanical properties of the P(AAm-co-HMA)-CL hydrogels became poor. Therefore, an optimum CL content and HMA/AAm molar ratio resulted in excellent mechanical properties of P(AAm-co-HMA)-CL hydrogels with an appropriate cross-linking density.

Conclusions

In this work, a series of cationic PMMA latex particles with different sizes were synthesized. Then, a series of P(AAm-co-HMA)-CL hydrogels were prepared by introducing the cationic PMMA latex particles of different sizes as the dynamic hydrophobic cross-linking centers. As cross-linking centers, CL played an important role in the hydrogel system. The size of CL had a significant effect on the mechanical and self-recovery properties of the P(AAm-co-HMA)-CL hydrogels. The degree of entanglement of the hydrophobic chains was different on the surface of CL with different sizes. The smaller size of CL was more conducive to the hydrophobic chain entanglement. Hence, the hydrogels with small sizes of CL had better mechanical and self-recovery properties. The tensile strength and toughness of P(AAm-co-HMA)-CL hydrogel could reach up to 1.47 MPa and 11.72 MJ m^{-3}. In addition, the mechanical properties of P(AAm-co-HMA)-CL hydrogel could be tuned by adjusting the CL content and HMA/AAm molar ratio. Therefore, the current study may provide novel avenues and theoretical support for the design of hydrogels toughened with latex particles and further expand the applications of hydrogels.

Conflicts of interest

There are no conflicts to declare.
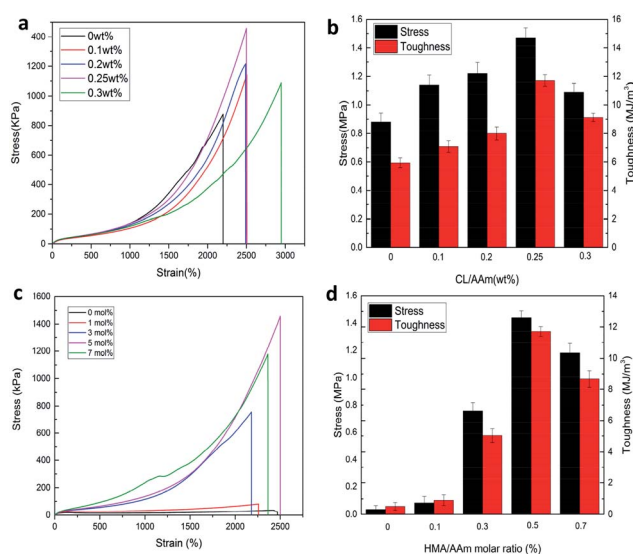
Acknowledgements

Fig. 9 (a) Tensile curve and (b) toughness of P(AAm-co-HMA)-CL hydrogel with different CL concents; (c) tensile curve and (d) toughness of P(AAm-co-HMA)-CL hydrogel with different HMA/AAm molar ratio.

References

1 X. J. Liu, H. Q. Li, B. Y. Zhang, Y. J. Wang, X. Y. Ren, S. Guan and G. Hui Gao, RSC Adv., 2016, 6, 4850–4857.

2 L. Wang, G. Shan and P. Pan, *Soft Matter*, 2014, **10**, 3850–3856.

3 K. Arakaki, N. Kitamura, H. Fujiki, T. Kurokawa, M. Iwamoto, M. Ueno, F. Kanaya, Y. Osada, J. P. Gong and K. Yasuda, *J. Biomed. Mater. Res., Part A*, 2010, **93**, 1160–1168.

4 B. G. Cooper, R. C. Stewart, D. Burstein, B. D. Snyder and M. W. Grinstaff, *Angew. Chem.*, 2016, **128**, 4298–4302.

5 T. Vermonden, R. Censi and W. E. Hennink, *Chem. Rev.*, 2012, **112**, 2853–2888.

6 J. L. Drury and D. J. Mooney, *Biomaterials*, 2003, **24**, 4337–4351.

7 S. H. Söntjens, D. L. Nettles, M. A. Carnahan, L. A. Setton and M. W. Grinstaff, *Biomacromolecules*, 2006, **7**, 310–316.

8 G. Gao, G. Du, Y. Sun and J. Fu, *ACS Appl. Mater. Interfaces*, 2015, **7**, 5029–5037.

9 M. Liu, W. Li, J. Rong and C. Zho, *Colloid Polym. Sci.*, 2012, **290**, 895–905.

10 J. Yang, X.-P. Wang and X.-M. Xie, *Soft Matter*, 2012, **8**, 1058–1063.

11 C. Katsuno, A. Konda, K. Urayama, T. Takigawa, M. Kidowaki and K. Ito, *Adv. Mater.*, 2013, **25**, 4636–4640.

12 T. Sakai, T. Matsunaga, Y. Yamamoto, C. Ito, R. Yoshida, S. Suzuki, N. Sasaki, M. Shibayama and U.-i. Chung, *Macromolecules*, 2008, **41**, 5379–5384.

13 H. Kamata, Y. Akagi, Y. Kayasuga-Kariya, U. I. Chung and T. Saka, *Science*, 2014, **343**, 873–875.

14 F. Jiang, T. Huang, C. He, H. R. Brown and H. Wang, *J. Phys. Chem. B*, 2013, **117**, 13679–13687.

15 J. Zhao, K. Jiao, J. Yang, C. He and H. Wang, *Polymer*, 2013, **54**, 1596–1602.

16 X. Li, C. Wu, Q. Yang, S. Long and C. Wu, *Soft Matter*, 2015, **11**, 3022–3033.

17 Q. Wang, R. Hou, Y. Cheng and J. Fu, *Soft Matter*, 2012, **8**, 6048.

18 J. P. Gong, Y. Katsuyama, T. Kurokawa and Y. Osada, *Adv. Mater.*, 2003, **15**, 1155–1158.

19 T. Huang, H. Xu, K. Jiao, L. Zhu, H. R. Brown and H. Wang, *Adv. Mater.*, 2007, **19**, 1622–1626.

20 Y. Wu, Z. Zhou, Q. Fan, L. Chen and M. Zhu, *Mater. Chem.*, 2009, **19**, 7340–7346.

21 X. Ren, C. Huang, L. Duan, B. Liu, L. Bu, S. Guan, J. Hou, H. Zhang and G. Gao, *Soft Mater.*, 2017, **13**, 3352–3358.

22 S. Xia, S. Song, X. Ren and G. Gao, *Soft Matter*, 2017, **13**, 6059–6067.

23 S. Gu, L. Duan, X. Ren and G. H. Gao, *J. Colloid Interface Sci.*, 2017, **492**, 119–126.

24 J. Hou, X. Ren, S. Guan, L. Duan, G. H. Gao, Y. Kuai and H. Zhang, *Soft Matter*, 2017, **13**, 1357–1363.

25 Y. Gao, L. Duan, S. Guan, G. Gao, Y. Cheng, X. Ren and Y. Wang, *RSC Adv.*, 2017, **7**, 44673.

26 X. Zhao, *Soft Matter*, 2014, **10**, 672–687.

27 M. Zhong, Y. T. Liu, X. Y. Liu, F. K. Shi, L. Q. Zhang, M. F. Zhu and X. M. Xie, *Soft Matter*, 2016, **12**, 5420–5428.